A Section 508–conformant HTML version of this article is available at https://doi.org/10.1289/EHP6993.

Profiling the Tox21 Chemical Collection for Acetylcholinesterase Inhibition

Shuaizhang Li,[1] Jinghua Zhao,[1] Ruili Huang,[1] Jameson Travers,[1] Carleen Klumpp-Thomas,[1] Wenbo Yu,[2] Alexander D. MacKerell Jr.,[2] Srilatha Sakamuru,[1] Masato Ooka,[1] Fengtian Xue,[2] Nisha S. Sipes,[3] Jui-Hua Hsieh,[3] Kristen Ryan,[3] Anton Simeonov,[1] Michael F. Santillo,[4] and Menghang Xia[1]

[1]Division for Pre-Clinical Innovation, National Center for Advancing Translational Sciences, National Institutes of Health, Rockville, Maryland, USA
[2]Department of Pharmaceutical Sciences, University of Maryland, Baltimore, Maryland, USA
[3]Division of the National Toxicology Program, National Institute of Environmental Health Sciences, National Institutes of Health, Research Triangle Park, North Carolina, USA
[4]Division of Toxicology, Office of Applied Research and Safety Assessment, Center for Food Safety and Applied Nutrition, U.S. Food and Drug Administration, Laurel, Maryland, USA

Background: Inhibition of acetylcholinesterase (AChE), a biomarker of organophosphorous and carbamate exposure in environmental and occupational human health, has been commonly used to identify potential safety liabilities. So far, many environmental chemicals, including drug candidates, food additives, and industrial chemicals, have not been thoroughly evaluated for their inhibitory effects on AChE activity. AChE inhibitors can have therapeutic applications (e.g., tacrine and donepezil) or neurotoxic consequences (e.g., insecticides and nerve agents).

Objectives: The objective of the current study was to identify environmental chemicals that inhibit AChE activity using *in vitro* and *in silico* models.

Methods: To identify AChE inhibitors rapidly and efficiently, we have screened the Toxicology in the 21st Century (Tox21) 10K compound library in a quantitative high-throughput screening (qHTS) platform by using the homogenous cell-based AChE inhibition assay and enzyme-based AChE inhibition assays (with or without microsomes). AChE inhibitors identified from the primary screening were further tested in monolayer or spheroid formed by SH-SY5Y and neural stem cell models. The inhibition and binding modes of these identified compounds were studied with time-dependent enzyme-based AChE inhibition assay and molecular docking, respectively.

Results: A group of known AChE inhibitors, such as donepezil, ambenonium dichloride, and tacrine hydrochloride, as well as many previously unreported AChE inhibitors, such as chelerythrine chloride and cilostazol, were identified in this study. Many of these compounds, such as pyrazophos, phosalone, and triazophos, needed metabolic activation. This study identified both reversible (e.g., donepezil and tacrine) and irreversible inhibitors (e.g., chlorpyrifos and bromophos-ethyl). Molecular docking analyses were performed to explain the relative inhibitory potency of selected compounds.

Conclusions: Our tiered qHTS approach allowed us to generate a robust and reliable data set to evaluate large sets of environmental compounds for their AChE inhibitory activity. https://doi.org/10.1289/EHP6993

Background

Acetylcholinesterase (AChE, acetylcholine acetylhydrolase, E.C. 3.1.1.7), located at the neuromuscular junctions and cholinergic nerve synapses, is involved in neurotransmission termination by hydrolysis of acetylcholine (ACh) into choline (Colović et al. 2013; Massoulié et al. 1993). Inhibition of AChE can lead to acetylcholine accumulation, hyperstimulation of nicotinic and muscarinic receptors, and disrupted neurotransmission. Depending on the scenario, AChE inhibitors can be toxic or have human therapeutic applications (Pohanka 2011). Although inhibition of AChE activity is an important therapeutic mechanism of action for disease treatments [e.g., Alzheimer's disease (AD), myasthenia gravis, and glaucoma], inhibition of AChE activity can cause cholinergic crisis, which is a collection of adverse health effects (Almasieh et al. 2013; Ohbe et al. 2018). Some examples of AChE inhibitors that cause adverse effects include pesticides, chemical warfare agents, drugs, and phytochemicals (Colović et al. 2013; Mukherjee et al. 2007). AChE inhibition measurement has been commonly used as a biomarker of organophosphorous and carbamate exposure in environmental and occupational human health (Farahat et al. 2011; Suarez-Lopez et al. 2013). In fact, AChE is one of several targets routinely tested by the pharmaceutical industry in early safety pharmacology studies (Bowes et al. 2012) used to identify potential safety liabilities. In addition to these recognized functions of AChE, there is emerging evidence that AChE is involved in other "nonclassical" cellular mechanisms (Soreq and Seidman 2001), such as apoptosis (Du et al. 2015), and cancer (Battisti et al. 2009; Castillo-González et al. 2015; Martínez-Moreno et al. 2006; Montenegro et al. 2006; Zhao et al. 2011). Therefore, identifying compounds that inhibit AChE activity is important for not only drug discovery but also for identifying potential chemical hazards that can adversely affect human health. To date, there are many compounds that have not been thoroughly evaluated for their effects on AChE activity, including drug candidates, food additives, industrial chemicals, and compounds relevant to environmental health.

Toxicology in the 21st Century (Tox21) is a federal collaboration among the U.S. Environmental Protection Agency (EPA), National Toxicology Program (NTP), National Center for Advancing Translational Sciences (NCATS), and the Food and Drug Administration (FDA). Tox21 focuses on development and application of *in vitro* high-throughput screening (HTS) for prioritizing chemicals for deeper toxicological evaluations, identifying mechanisms of chemicals-induced biological activity, and developing models for predicting *in vivo* responses (Krewski et al. 2009; Tice et al. 2013). The Tox21 compound library contains approximately 10,000 (10K) chemicals, which include, for example, approved drugs and environmental chemicals (Attene-Ramos et al. 2013). Tox21 has generated nearly 100 million data points

Address correspondence to Menghang Xia, National Institutes of Health, National Center for Advancing Translational Sciences, 9800 Medical Center Dr., Rockville, MD 20892-3375 USA. Telephone: (301) 827-5359. Email: mxia@mail.nih.gov

Supplemental Material is available online (https://doi.org/10.1289/EHP6993).
The authors declare they have no actual or potential competing financial interests.
Received 2 March 2020; Revised 1 March 2021; Accepted 9 March 2021; Published 12 April 2021.

using *in vitro* HTS assays (Tice et al. 2013). Tox21 data in combination with chemical structure information produced robust predictive models for human toxicity end points (Huang et al. 2016). Tox21 expands the focus of its research activities continuously, including improvement of current *in vitro* test systems, development of new alternative test systems, and refining alternative methods for characterizing pharmacokinetics and *in vitro* assay disposition in *in vivo* toxicity testing data curation (Thomas et al. 2018).

To identify environmental chemicals that inhibit the enzymatic activity of AChE, we screened the Tox21 10K compound library using three quantitative HTS (qHTS) assays: a cell-based (SH-SY5Y) AChE assay, an enzyme-based (recombinant human AChE) AChE inhibition assays without microsomes, and the same enzyme-based assay with microsomes.

Materials and Methods

Materials

Human neuroblastoma cells (SH-SY5Y), F12, and Eagle's minimum essential media were obtained from American Type Culture Collection. StemPro® Neural Stem Cells, and StemPro® NSC SFM were obtained from Thermo Fisher Scientific. HyClone™ fetal bovine serum (FBS) was obtained from Life Sciences/GE Health care. Amplite colorimetric AChE assay kit was purchased from AAT Bioquest, Inc. Chlorpyrifos-oxon was purchased from Chem Service, Inc. Chlorpyrifos, BW284c51, β-Nicotinamide adenine dinucleotide 2′-phosphate (NADPH), dimethyl sulfoxide (DMSO), and purified recombinant human AChE protein were purchased from Sigma-Aldrich. InVitroCYP 150-D human liver microsomes (HLM), prepared from 150 donor human liver tissue fraction pools with mixed gender, were purchased from BIOIVT. The Tox21 10K compound library was provided by the Tox21 program, and its information was described in a recent publication (Richard et al. 2020). The list of the Tox21 10K compounds can be found at https://tripod.nih.gov/tox21/assays/download/tox21_10k_library_info.tsv.zip (also listed in Excel Table S1).

Cell Culture

Human SH-SY5Y cells were cultured in a mixture of Eagle's minimum essential medium (45%), F-12 medium (45%), supplemented with 10% FBS (HyClone Laboratories) and 50 U/mL penicillin and 50 μg/mL streptomycin. The cells were maintained at 37°C under a humidified atmosphere and 5% CO_2. StemPro® Neural Stem Cells (NSC) are cryopreserved human fetal brain–derived neural stem cells (NSCs) and were cultured in complete medium, including KnockOut D-MEM/F-12, StemPro® Neural Supplement, basic fibroblast growth factor (bFGF), epidermal growth factor (EGF), and GlutaMAX™-I Supplement. NSCs were cultured in Matrigel®-coated flasks and maintained at 37°C and 5% CO_2. For the adhesion of NSCs to the microplate, the cell suspension was mixed with vitronectin at 1:100 dilution.

AChE Inhibition Assays in qHTS Screening

Three colorimetric AChE inhibition assays, cell-, and enzyme-based with or without microsomes, were described previously (Li et al. 2017, 2019). All the primary screening assays were run in the robotic platform (Attene-Ramos et al. 2013). Briefly, SH-SY5Y cells (2,000 cells per well) for cell-based AChE assay or recombinant human AChE (50 mU/mL, with or without 0.25 mg/mL microsomes) for enzyme-based assay were dispensed (4 μL per well without microsomes addition and 3 μL per well with microsomes plus 1 μL of NADPH) into black/clear bottom 1,536-well plates. For the cell-based assay, cells were cultured overnight. Heat-inactivated microsomes used in the enzyme-based assay for follow-up studies were used as a control for protein binding. Test compounds (final concentration range from 0.74 nM to 57.6 μM) or positive and negative (DMSO, 0.58% in the assay well) controls (23 nL) were transferred into the assay plates using a Wako Pintool station, and the assay plates were incubated for 30 min at room temperature. Chlorpyrifos-oxon at concentrations ranging from 88 pM to 2.88 μM and BW284c51 at concentrations ranging from 0.88 nM to 28.8 μM were used as the positive controls in cell-based assay and enzyme-based assay without microsomes, whereas chlorpyrifos ranging from 3.5 nM to 112 μM was used as a positive control in enzyme-based assay with microsomes. Next, 4 μL of colormetric detection cocktail solution [5,5'-dithio-*bis*-(2-nitrobenzoic acid) (DTNB), acetylthiocholine] was added to each well using a BioRAPTR™ FRD™. Assay plates were incubated for 30 min at room temperature, followed by measuring absorbance (ex = 405 nm), using an Envision plate reader. The metabolic active AChE inhibitors were defined by the differences of their half-maximal inhibitory concentration [IC_{50} values (≥3-fold) between assays with and without microsomes].

AChE Inhibition Assays in Spheroids

The 1,536-well microplates were used to form spheroids. The microplates feature black/opaque walls, round well-bottom geometry with ultra-low attachment surface. SH-SY5Y cells or neural stem cells (2,000 cells per well) were plated into the spheroid plates. The plates were then centrifuged for 5 min at 1,500 rpm to aggregate cells, and thereafter plates were cultured at 37°C, 5% CO_2 for 24 h or 48 h. The addition of test compounds and AChE inhibition assay was performed as mentioned in the previous section. Each compound was tested in three experiments.

Cell-Based P450-Glo Induction Assays in 96-Well Plate

P450-Glo CYP3A4, CYP1A2, CYP2B6, and CYP2D6 assay kits were purchased from Promega Corporation. Spheroid 96-well microplates used for the growth of 3D cell spheroid cultures and the black wall/clear bottom 96-well plates were purchased from Corning Life Sciences. The positive controls for induction assays were purchased from Sigma-Aldrich. SH-SY5Y and neural stem cells were plated at 30,000 per well in 80 μL of the culture medium in black wall/clear bottom 96-well or spheroid 96-well plates. The assay plates were incubated at 37°C for 48 h. For induction assays, 10 μL of omeprazole (CYP1A2) or rifampicin (CYP2B6, CYP2D6, and CYP3A4) with eight concentrations ranging from 21 nM to 46 μM were transferred to the assay plates. After the assay plates were incubated at 37°C for 24 h, 10 μL P450-Glo substrates [3 μM Luc-IPA (3A4); 10 μM Luc-ME EGE (2D6); 6 μM Luc-1A2; 3 μM Luc-2B6] were added to assay wells. The assay plates were incubated at 37°C for an additional 1 h. The reactions were stopped by the addition of 100 μL P450-Glo detection reagents for each assay. After 20 min incubation at room temperature, the luminescence intensity was quantified using ViewLux™ plate reader. Data were expressed as relative luminescence units. Each data point represents the mean ± standard deviation (SD) of three experiments.

Real-Time Reverse Transcription Polymerase Chain Reaction (RT-PCR)

Neural stem cells and SH-SY5Y cells were plated at 30,000 cells per well in the 96-well plates, and then incubated either in monolayer or spheroid format. After 2-d incubation, these cells were washed with PBS twice. Cells from 20 wells were combined and

harvested with lysis buffer from RNeasy Mini Kit. The total RNAs were extracted from these cells using RNeasy Mini Kit, and their RNA concentrations were determined with NanoDrop™. A total of 25 ng of total RNA from each sample was used to perform the RT-PCR with Power SYBR™ Green RNA-to-C_T C_T™ 1-Step Kit. Total volume for each reaction was 20 μL with final primer concentration of 150 nM for CYP3A4, CYP2D6, CYP1A2, and CYP2B6. GAPDH was used as a control. The real-time PCR reactions (1 cycle 95°C 10 min for Taq polymerase activation and 40 cycles 95°C 15 s and 60°C 1 min for annealing/extension) were run on a QuantStudio™ 3 Real-Time PCR System according to the manufacturer's instructions. All the primers were purchased from MilliporeSigma. The primer sequences were listed as follows: CYP1A2, 5′-CACTATCAGGACTTTGACAAG-3′ and 5′-AGGTTGACAATCTTCTCCTG-3′; CYP2B6, 5′-AGGTTCCGAGAGAAATATGG-3′ and 5′-TTTCCATTGGCAAAGATCAC-3′; CYP3A4, 5′-AGTCTTTCCATTCCTCATCC-3′ and 5′-TGCTTTTGTGTATCTTCGAG-3′; CYP2D6, 5′-CCTATGAGCTTTGTGCTG-3′ and 5′-TTTGGAACTACCACATTGC-3′; GAPDH, 5′-TCGGAGTCAACGGATTTG-3′ and 5′-CAACAATATCCACTTTACCAGAG-3′. The number of cycle threshold (Ct) of each reaction was determined. Induction values were calculated using the following equation: $\text{Fold} = 2^{-\Delta\Delta Ct}$, where ΔCt represents the differences in cycle threshold numbers between CYP3A4, CYP2B6, CYP1A2 or CYP2B6 and GAPDH, and ΔΔCt represents the relative change in these differences between monolayer and spheroid groups.

Reversible and Irreversible Experiment of AChE Inhibitors

Recombinant human AChE (100 mU/mL) was dispensed at 4 μL per well into black/clear bottom 1,536-well plates using a Multidrop™ Combi 8-channel dispenser. Twenty-three nanoliters of test compounds, positive controls, chlorpyrifos-oxon (88 pM to 2.88 μM), and BW284c51 (0.88 nM to 28.8 μM), or negative control (DMSO, 0.58% in the assay well), were transferred into the assay plates using a Wako Pintool station, and the assay plates were incubated for 5 min, 10 min, and 60 min at room temperature. The addition of test compounds and AChE inhibition assay was performed as mentioned in the "Materials and Methods" section, "AChE Inhibition Assays in qHTS Screening." Each compound was tested three times at different time points. The compounds were considered as irreversible if there was a statistically significant difference between the IC_{50} values of different time points (10 min vs. 5 min, 60 min vs. 5 min) [one-way analysis of variance (ANOVA) test, $p < 0.05$], whereas compounds were considered reversible if there was no statistically significant difference between IC_{50S} at different time points ($p > 0.05$).

qHTS Assay Data Analysis

Analysis of compound concentration–response data was performed as described previously (Huang 2016; Inglese et al. 2006). First, raw plate readings for each titration point were normalized relative to the positive control compound (chlorpyrifos-oxon and BW284c51 for cell- and enzyme-based assays, respectively; −100%) and DMSO-only wells (0%) according to the following calculation: $\%\,\text{Activity} = [(\text{Vcompound} - V_{DMSO})/(V_{DMSO} - \text{Vpos})] \times 100$, where Vcompound represents compound well values. The median well values of the positive control and DMSO are represented by Vpos and V_{DMSO}, respectively. An in-house pattern correction algorithm was applied to the data set using the DMSO-only compound plates at the beginning and end of the compound plate stack (Wang and Huang 2016). To obtain each compound's half maximum inhibition value (IC_{50}) and maximum response (efficacy) value, concentration–response curves of each compound were fitted to a four-parameter Hill equation (Wang et al. 2010). Compounds received a class designation between 1 and 4, depending on the type of concentration–response curve observed (Inglese et al. 2006). Curve classes are heuristic measures of data confidence, classifying concentration–responses based on efficacy, the number of data points observed above background activity, and the quality of fit (Huang et al. 2011). The number of significant data points, i.e., data points with significantly higher than background activity, determines the four major classes: Class 1 (complete) and Class 2 (incomplete) curves have more than one significant point, Class 3 curves have only one significant point, and Class 4 curves have no significant point. Class 1 and Class 2 curves are further divided into four subcategories, based on quality of fit and efficacy: Curves with good fit are classified as x.1 (full efficacy) and x.2 (partial efficacy), and curves with poor fit are classified as x.3 (full efficacy) and x.4 (partial efficacy). In addition, activators are assigned positive curve classes and inhibitors are assigned negative curve classes. Compounds that inhibited AChE activity were defined as antagonists in the study. Compounds with Class −1.1, −1.2, −2.1, or −2.2 (efficacy $< -50\%$) label curves were considered active, and compounds with Class 4 label curves were considered inactive. Remaining compounds with all other curve classes were considered inconclusive. Potential AChE inhibitors were selected from compounds active in either the cell-based assay or the enzyme-based assay with or without microsomes. In addition, the enzyme-based assay with microsomes was used to identify compounds that needed metabolic activation. Only compounds that passed the chemical quality control test for identity (confirmed by molecular weight) and purity (>75%) were selected for confirmation and follow-up studies, and these chemical quality control data were directly obtained from the Tox21 program at https://tripod.nih.gov/tox21/samples (27 March 2021). Data were further analyzed (e.g., *t*-test, and one-way ANOVA test) and depicted using GraphPad Prism 5 (GraphPad Software, Inc.).

Chemical Structure-Activity Cluster Analysis

The Tox21 10K compound collection was grouped into 1,014 clusters based on structural similarity (9,242-bit fingerprints; Leadscope®) using the self-organizing map (SOM) algorithm (Attene-Ramos et al. 2013; Kohonen 2006). Fingerprints are digital representations of chemical structures. A fingerprint of a chemical is a bit vector composed of ones and zeros, with each bit representing a structural feature. A bit is set to 1 if the corresponding feature is present in the chemical and to 0 if the feature is absent. Each cluster was evaluated for its enrichment of active AChE inhibitors by comparing the fraction of actives in the cluster with the fraction of actives not in the cluster. A cluster is considered enriched with actives if the former fraction is larger than the latter. The significance of enrichment was determined by the Fisher's exact test ($p < 0.01$).

Molecular Docking

Molecular docking was used to study the binding modes of AChE inhibitors. Simulations began with the X-ray crystal structure of the target protein AChE (PDB 4EY7) without the small molecule inhibitor donepezil. Site identification by ligand competitive saturation (SILCS) simulations and analysis were conducted using the MolCal program, scripts (SilcsBio, LLC.) (Guvench and MacKerell 2009; Raman et al. 2013; Ustach et al. 2019), and GROMACS simulation program (Hess et al. 2008). Specifically, a series of SILCS simulations were set up by following our previously reported protocols (Lakkaraju et al. 2015; Raman et al. 2013), employing Grand-Canonical Monte Carlo

(GCMC) and molecular dynamics (MD) in an iterative fashion. GCMC samples water molecules and different types of solutes followed by MD simulation. The iterative GCMC–MD process enables conformational dynamics sampling of AChE, solutes, and water molecules (Lakkaraju et al. 2015). In the simulations, the CHARMM36 protein force field (Huang et al. 2017) was used to describe the AChE protein, CHARMM TIP3P model (Neria et al. 1996) for water molecules, and CHARMM General Force Field (CGenFF) for the solute molecules and inhibitors (Vanommeslaeghe et al. 2010; Yu et al. 2012). To dock the selected inhibitors to the active site of AChE, Monte Carlo sampling using the SILCS [SILCS-Monte Carlo (MC)] protocol (Raman et al. 2013) was performed to predict compound binding modes. The binding affinities were evaluated by the Ligand Grid Free Energy (LGFE) (Lakkaraju et al. 2015; Raman et al. 2013). In the current study for visualization and scoring, a series of FragMaps were used to represent different types of functionalities, including generic apolar (benzene, propane), generic H-bond donor [methanol O, formamide N, imidazole (NH)], and generic H-bond acceptor (methanol O, formamide O, imidazole N, acetaldehyde O), negatively charged (acetate), and positively charged (methylammonium). Sulfur atoms in compounds were treated as apolar groups. For each compound, five independent runs of SILCS-MC were completed, where each run entailed multiple SILCS-MC cycles performed in a two-step fashion. The first stage of each cycle involves 10,000 Metropolis MC steps that sample a broad range of binding poses with a 180-degree step size for overall rotations, 1 Å for translations, and 180 degrees for dihedral angle rotations, at 298 K. The second part of the cycle includes 40,000 steps of MC simulated annealing (SA) that are designed to identify a local minimum within the acceptance criteria defined by the LGFE. SA allows maximum step size range of 9 degrees for overall rotations, 0.2 Å for translations, and 9 degrees for dihedral angle rotations with a temperature range between 298 and 0 K. The five SILCS-MC runs involved multiple MC cycles each initiated with a random seed and continued until the three most favorable LGFE scores were within 0.5 kcal/mol (50–250 cycles performed). The docking pose with the most favorable LGFE value was reported as the predicted binding mode of a ligand.

Results

Identification of Compounds That Inhibit AChE Activity

Cell (i.e., SH-SY5Y line)- and enzyme-based (with or without microsomes) AChE inhibition assays were used to screen the Tox21 10K compound collection containing 8,312 unique chemicals [deposited in PubChem Bioassay Database; IDs 1347395, 1347397, 1347399]. Of these 8,312 unique compounds tested, 187 (2.25%) decreased the AChE activity with efficacy more than 50% or compounds with class −1.1, −1.2, −2.1, or −2.2 (efficacy $< -50\%$) (Figure 1; Excel Table S2 and S3). From the primary screening and confirmation testing (Excel Table S3), 111 compounds were selected for further follow-up studies based on efficacy (>50%) and IC_{50} (<20 μM). The 111 compounds that inhibited AChE activity had IC_{50} values ranging from 1 nM to 20 μM, and 19 compounds with an $IC_{50} < 1$ μM (Table S1). Of the 111 compounds, 104 compounds were confirmed to be active in cell- or enzyme-based AChE assay with 100 compounds active in both assays, and 7 inactive compounds were active after incubation with human microsomes (Figure S1). The IC_{50} values of all these compounds were listed in Table S2 (see raw data in Excel Table S4). Many previously reported AChE inhibitors, including pesticides and drugs such as carbofuran, tacrine, ambenonium, and physostigmine, were identified in our study.

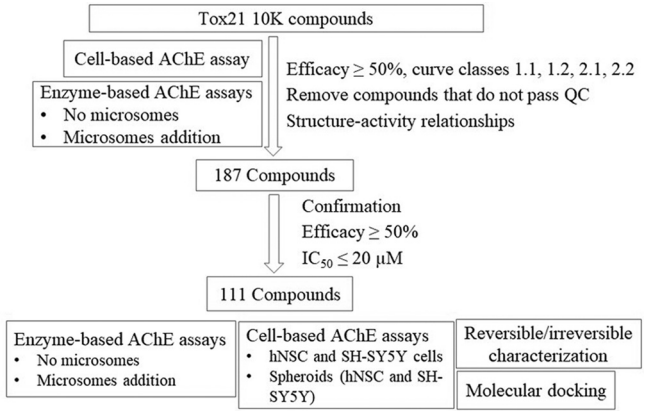

Figure 1. Screening and compound prioritization workflow. Cell-based and enzyme-based assays were developed for screening AChE inhibitors, and enzyme-based assay with metabolic activation was also included to screen inhibitors. After primary concentration–response screenings, in which each compound was tested at 15 concentrations, 187 compounds were identified based on potency and efficacy. A total of 187 compounds were tested in the follow-up studies. Based on efficacy and IC_{50}, 111 compounds were selected for further studies.

Ambenonium chloride, a previously reported AChE inhibitor, was the most potent compound, with an IC_{50} of 1 nM. Many potential novel AChE inhibitors (including pesticides and drugs), such as azasetron hydrochloride, tilorone, orlistat, and eperisone hydrochloride, were identified from our enzyme-based screenings with IC_{50} values of 7.22 μM, 4.18 μM, 1.59 μM, and 27.4 μM respectively (Table 1). The concentration response curves of these compounds are shown in Figure S2. The chemical structures for potential novel AChE inhibitors identified from the current study are presented in Figure S3. These compounds represent a variety of structural scaffolds, molecular weights, and functional groups.

Structure-Activity Relationships (SAR) of AChE Inhibitors

The Tox21 10K compound library was clustered based on their structural similarity using the SOM algorithm (Kohonen 2006), yielding 1,014 clusters. Each cluster was evaluated for the enrichment of active AChE inhibitors based on the cell-based and enzyme-based assay results (Figure 2, Excel Table S5). Thirty and 35 clusters were found significantly ($p < 0.01$) enriched with AChE inhibitors based on the enzyme- and cell-based assays, respectively. One cluster significantly enriched with active inhibitors (Figure 2, row 9, column 22, $p = 4.57 \times 10^{-11}$) contained a group of 21 carbamate compounds that included aldicarb, carbaryl, and methomyl, which were previously reported AChE inhibitors. Other significant clusters containing previously reported AChE inhibitors, including organophosphates (OP) (chlorpyrifos, chlorpyrifos-oxon, and isazofos) and acridines (9-aminoacridine, hydroxytacrine maleate, and tacrine), were also confirmed in our study. Additionally, a cluster of compounds containing tilorone, raloxifene hydrochloride, and moxisylyte was found to be significantly enriched in compounds not previously identified as AChE inhibitors, but they were identified in the current study (Figure 2, row 7, column 26, $p = 1.32 \times 10^{-7}$). Moreover, blue dyes (Figure 2, row 42, column 8) including methylene blue and toluidine blue were identified in our study as AChE inhibitors.

Identification of AChE Inhibitors via Metabolic Activation

Some organophosphorus pesticides (OPs) are not active AChE inhibitors in their parental form, but become active through metabolism (Sultatos 1994). To identify the AChE inhibitors that

Table 1. Potency and efficacy values of potential novel AChE inhibitors.

Compounds	Enzyme	Enzyme with microsomes	SH-SY5Y cells monolayer	SH-SY5Y spheroids (24 h)	SH-SY5Y spheroids (48 h)	Neural stem cells monolayer	Neural stem cell spheroid (24 h)	Neural stem cell spheroid (48 h)
Amisulpride	14.35 ± 2.58 (−90.26 ± 8.4)	21.76 ± 2.5 (−71.97 ± 2.19)	30.74 ± 3.53 (−45.91 ± 3.28)	11.13 ± 7.28 (−92.81 ± 1.02)	28.65 ± 5.15 (−53.05 ± 7.1)	17.22 ± 6.14 (−52.29 ± 5.13)	Inactive	12.14 ± 10.38 (−21.95 ± 5.43)
Azasetron hydrochloride	7.72 ± 0.88 (−61.3 ± 1.86)	8.97 ± 0.6 (−37.31 ± 7.07)	6.6 ± 0.43 (−70.85 ± 15.38)	9.64 ± 8.85 (−96.01 ± 32.13)	6.85 ± 0 (−66.91 ± 7.49)	6.88 ± 0.79 (−67.84 ± 4.01)	16.49 ± 3.98 (−77.98 ± 5.01)	18.78 ± 3.2 (−74.29 ± 20.2)
Azelastine (hydrochloride)	25.41 ± 3.23 (−32.35 ± 9.86)	27.4 ± 3.14 (−15.8 ± 6.37)	20.88 ± 1.36 (−64.6 ± 5.15)	13.82 ± 11.61 (−69.46 ± 18.33)	19.31 ± 0 (−66.42 ± 12.17)	22.55 ± 1.52 (−52.77 ± 4.94)	Inactive	4.45 ± 5.91 (−15.14 ± 86.34)
Bromopride	19.4 ± 2.22 (−83.78 ± 4.74)	22.55 ± 1.52 (−64.15 ± 5.04)	8.43 ± 3.43 (−55.58 ± 7.34)	3.63 ± 3.8 (−96.83 ± 18.51)	20.28 ± 3.65 (−69.27 ± 7.32)	3.9 ± 0.81 (−101.84 ± 4.1)	1.11 ± 0.31 (−63.61 ± 16.97)	0.58 ± 0.13 (−59.82 ± 3.4)
Chlorhexidine diacetate	54.57 ± 13.62 (−79.28 ± 11.59)	Inactive	70.89 ± 13.24 (−51.61 ± 11.08)	36.12 ± 10.06 (−75.23 ± 14.14)	40.97 ± 2.77 (−54.9 ± 2.8)	32.53 ± 2.2 (−81.17 ± 1.38)	8.31 ± 1.87 (−70.72 ± 16.06)	9.21 ± 1.17 (−72.08 ± 16.96)
Ecopipam	20.1 ± 1.36 (−60.34 ± 13.31)	27.28 ± 0 (−34.87 ± 7.48)	15.75 ± 6.17 (−32.9 ± 4.14)	Inactive	17.72 ± 4.94 (−42.52 ± 6.77)	17.51 ± 4 (−72.51 ± 8.83)	Inactive	3.16 ± 2.24 (−36.48 ± 8.2)
Eperisone hydrochloride	27.4 ± 3.14 (−57.18 ± 4.43)	38.7 ± 4.44 (−59.36 ± 2.47)	25.3 ± 1.71 (−71.01 ± 2.24)	13.8 ± 10.44 (−45.01 ± 20.24)	32.6 ± 9.21 (−66.41 ± 3.82)	19.31 ± 0 (−94.25 ± 1.82)	14.99 ± 10.82 (−69.46 ± 16.49)	13.29 ± 2.26 (−62.36 ± 14.7)
GW473178E methyl benzene sulfonic acid	10.62 ± 0.69 (−91.11 ± 1.43)	18.89 ± 1.23 (−96.61 ± 7.64)	23.27 ± 5.25 (−88.9 ± 10.7)	9.63 ± 8.76 (−92.9 ± 16.03)	23.99 ± 4.09 (−89.53 ± 3.66)	24.78 ± 2.84 (−88.83 ± 7.19)	Inactive	31.2 ± 3.59 (−45.21 ± 8.8)
Hexachlorophene	14.91 ± 2.54 (−101.18 ± 7.69)	Inactive	Inactive	Inactive	Inactive	Inactive	Inactive	Inactive
Meptazinol hydrochloride	6.63 ± 1.23 (−72.59 ± 7.81)	8.91 ± 0.58 (−59.69 ± 4.61)	7.64 ± 0.51 (−85.78 ± 5.21)	5.14 ± 3.81 (−98.48 ± 12.69)	7.35 ± 0 (−80.08 ± 15.09)	6.47 ± 1.8 (−80.43 ± 6.83)	8.24 ± 0 (−82.96 ± 0)	7.89 ± 5.31 (−53.51 ± 18.57)
Moxisylyte hydrochloride	21.94 ± 4.1 (−22.04 ± 2.77)	19.31 ± 0 (−81.53 ± 5.5)	20.1 ± 1.36 (−76.34 ± 8.16)	14.35 ± 4.95 (−99.84 ± 2.13)	20.89 ± 1.36 (−71.64 ± 7.11)	19.31 ± 0 (−79.69 ± 5.13)	Inactive	24.32 ± 0 (−31.57 ± 0)
Orlistat	1.59 ± 0.79 (−58.45 ± 6.58)	12.24 ± 1.4 (−64.09 ± 8.33)	4.91 ± 0.91 (−46.87 ± 5.3)	9.46 ± 10.95 (−78.5 ± 4.49)	8.82 ± 6.03 (−32.01 ± 3.4)	3.44 ± 0.39 (−82.15 ± 3.93)	3.9 ± 1.5 (−53.61 ± 18.04)	2.36 ± 0.93 (−44.21 ± 5.87)
Rapacuronium bromide	22.64 ± 2.88 (−61.11 ± 3.7)	26.29 ± 1.71 (−57.14 ± 1.92)	16.03 ± 2.04 (−87.48 ± 6.36)	8.24 ± 7.11 (−53.26 ± 10.89)	22.55 ± 1.53 (−66.73 ± 3.11)	5.27 ± 0.72 (−90.03 ± 4.15)	3.64 ± 1.71 (−62.63 ± 15.19)	1.37 ± 0 (−58.33 ± 0)
Rhodamine 6G	22.83 ± 8.94 (−94.23 ± 4.33)	41.33 ± 5.26 (−82.16 ± 8.8)	12.36 ± 3.44 (−95.66 ± 7.4)	15.81 ± 1.81 (−114.21 ± 10.43)	9.25 ± 1.18 (−87.03 ± 4.89)	30.51 ± 14.33 (−93.03 ± 9.21)	29.7 ± 2.41 (−42.45 ± 2.64)	40.25 ± 9.21 (−42.47 ± 8.03)
Sulcaine	20.1 ± 1.36 (−58.05 ± 2.13)	23.43 ± 1.52 (−34.29 ± 3.66)	15.34 ± 0 (−72.75 ± 4.45)	12.89 ± 11.12 (−77.14 ± 33.35)	20.89 ± 1.36 (−66.79 ± 3.64)	19.56 ± 3.65 (−42.86 ± 5.64)	15.58 ± 12.34 (−28.44 ± 44.14)	13.67 ± 0 (−67.80 ± 0)
Tilorone	4.18 ± 0.57 (−92.77 ± 2.75)	5.46 ± 0.62 (−96.73 ± 6.07)	1.77 ± 0.49 (−102.93 ± 5.12)	1.34 ± 0.5 (−94.23 ± 7.77)	1.42 ± 0.1 (−90.98 ± 2.64)	5.88 ± 0.38 (−51.88 ± 0.98)	19.59 ± 13.98 (−34.23 ± 2.35)	25.74 ± 5.81 (−35.28 ± 13.55)

Note: Each value of potency (IC_{50}, μM) and efficacy (percent of positive control, expressed in parentheses) is the mean ± standard deviation (SD) of the results from three experiments. SH-SY5Y spheroids (24 h), SH-SY5Y spheroids (48 h), neural stem cell spheroids (24 h), or neural stem cell spheroids (48 h): AChE assays were performed after these cells were cultured in spheroid formation for 24 or 48 h. IC_{50}, concentration of half-maximal inhibition.

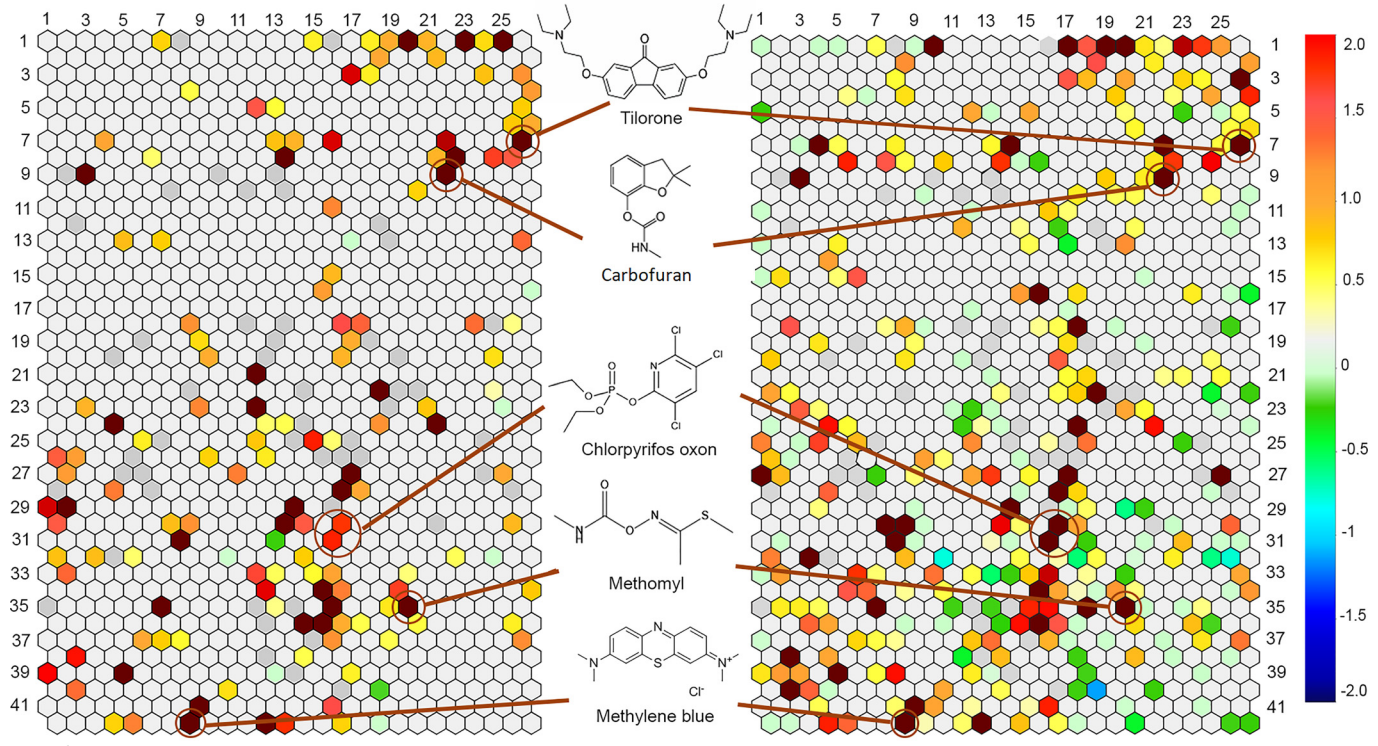

Figure 2. Structure clusters of the AChE inhibitors identified from enzyme-based assay (left) and cell-based assay (right). The Tox21 10K compound collection was clustered based on structural similarity. In the heat maps, each hexagon represents a cluster of structurally similar compounds. The color gradient is indicative of the enrichment of AChE inhibitors in that specific cluster [negative logarithmic scale of the *p*-value, -log (*p*-value)]. Clusters enriched with active inhibitors are closer to a maroon color, whereas clusters deficient of active inhibitors are colored in shades of blue or green. A light gray color indicates that the fraction of active inhibitors in that cluster is close to the library average. Empty clusters with no compounds in them are in a darker shade of gray. Each cluster was evaluated for its enrichment of active AChE inhibitors by comparing the fraction of actives in the cluster with the fraction of actives not in the cluster. The significance of enrichment was determined by the Fisher's exact test ($p < 0.01$).

need metabolic activation for their activity, we used an enzyme-based AChE inhibition assay with human microsomes. Of the 111 hits, 25 compounds were more potent for AChE inhibition after incubation with microsomes (the IC_{50} value differences were ≥3-fold between assays with and without microsomes) (Table 2). All 25 compounds are OP pesticides. Several compounds, such as carbophenothion, phosalone, and pyrazophos, were more potent AChE inhibitors after metabolism with IC_{50} values of 3.74 μM, 2.91 μM, and 7.89 μM (Figure 3; Excel Table S6). Some OP compounds, such as azamethiphos, chlorfenvinphos, diazinon, and dichlorvos, were potent AChE inhibitors in the absence of metabolic activation in our study. Several compounds, such as chlorpyrifos-oxon and ethyl 4-nitrophenyl ethylphosphonate, were less potent in inhibiting AChE in the presence of microsomes, most likely due to nonspecific protein binding, because similar results were observed with heat-inactivated microsomes (Tables S2 and S3; Excel Table S4). Many other compounds did not show IC_{50} differences (<3 fold) with microsomes addition.

Evaluation of AChE Inhibitors in Neural Stem Cells and Spheroids

To further investigate the activity of these 111 compounds found to inhibit AChE in SH-SY5Y cells, the human neural stem cells, which are a more physiologically relevant cell model, were also used to confirm these compounds have AChE inhibitory effect. In monolayer cultures of neural stem cells and SH-SY5Y cells, the IC_{50}s values of most AChE inhibitors (Table S2; Excel Tables S4 and S7) were comparable, except for bromophos-ethyl, phosalone, and quinalphos, which were more potent AChE inhibitors in neural stem cells (IC_{50} changes ≥3 fold). We also tested these 111 compounds in spheroids formed by SH-SY5Y and neural stem cell models (Excel Tables S8 and S9). Using SH-SY5Y cells, several compounds that included carbophenothion and phosalone were inactive AChE inhibitors in the monolayer cell culture but were active in the spheroids. In neural stem cells, some compounds, such as bromophos-ethyl, chlorpyrifos, and phosalone, were more potent in the spheroids than the monolayer cultures (Table 2). On the other hand, some compounds, like ambenonium chloride, chlorpyrifos-oxon, and donepezil hydrochloride, were more potent in monolayer cell culture than in the spheroids. Compounds like berberine, dyclonine, and imidocarb dipropionate did not show any difference in potency in monolayer cell culture and spheroids (Table S2).

To investigate which CYP enzyme isoforms were involved in monolayer cell culture vs. spheroids, P450-Glo assays were used to measure the induction of CYP3A4, CYP2D6, CYP1A2, and CYP2B6 in both monolayer and spheroid cultures for neural stem cells and SH-SY5Y cells. As shown in Supplemental Figure S4A and S4B (Excel Table S10), the induction of CYP3A4 and CYP2D6 by rifampicin was statistically significant in neural stem cell spheroids in comparison with monolayers. There was no difference of CYP3A4 and CYP2D6 induction between monolayer and spheroid of SH-SY5Y cells (Figure S4C and S4D; Excel Table S10). P450-Glo assays could not detect CYP1A2 and CYP2B6 for both neural stem cells and SH-SY5Y cells either in monolayers or spheroids. To further examine the gene expression of these four cyp isoforms, quantitative RT-PCR method was used. For neural stem cells, cyp3a4 and cyp2d6 expression was

Table 2. Potency and efficacy of compounds that inhibited AChE with an IC_{50} difference of ≥3-fold between assays conducted with and without microsomes.

Compounds	Enzyme	Enzyme with microsomes	SH-SY5Y cells monolayer	SH-SY5Y spheroids (24 h)	SH-SY5Y spheroids (48 h)	Neural stem cells monolayer	Neural stem cell spheroids (24 h)	Neural stem cell spheroids (48 h)
Azinphos-ethyl	42.76 ± 2.78 (−82.61 ± 4.51)	2.14 ± 0.13 (−92.25 ± 0.56)	10.93 ± 2.73 (−106.66 ± 2.68)	25.17 ± 14.26 (−115.13 ± 23.95)	12.05 ± 0.79 (−103.4 ± 2.65)	4.79 ± 0.31 (−108.94 ± 4.81)	2.23 ± 0.25 (−71.15 ± 13.32)	4.36 ± 1.09 (−56.29 ± 0.3)
Benfuracarb	4.97 ± 0 (−97.96 ± 1.1)	1.4 ± 0.16 (−96.37 ± 0.38)	1.25 ± 0.14 (−108.11 ± 5.64)	1.76 ± 1.52 (−126.84 ± 31.17)	0.84 ± 0.19 (−102.89 ± 8.1)	7.67 ± 1.3 (−134.56 ± 6.1)	12.15 ± 2.07 (−90.09 ± 19.27)	12.56 ± 1.44 (−74.65 ± 14.16)
Bromophos-ethyl	67.77 ± 4.41 (−53.43 ± 0.37)	5.66 ± 1.18 (−96.96 ± 2.35)	47.98 ± 3.12 (−62.26 ± 3.94)	37.36 ± 21.52 (−54.8 ± 9.22)	47.98 ± 3.13 (−66.18 ± 5.7)	11.47 ± 3.19 (−116.13 ± 5.75)	0.87 ± 0.21 (−70.93 ± 15.26)	1.99 ± 0.23 (−72.3 ± 16.09)
Carbophenothion	Inactive	3.74 ± 0.63 (−84.43 ± 2.03)	Inactive	28.06 ± 14.79 (−55.59 ± 44.65)	19.63 ± 13.26 (−29.69 ± 10.41)	2.96 ± 0.4 (−62.53 ± 2.18)	2.19 ± 0.41 (−70 ± 5.32)	3.31 ± 0.22 (−65.79 ± 9.3)
Carbosulfan	1.67 ± 0.72 (−89.8 ± 6.61)	0.44 ± 0.05 (−86.37 ± 1.31)	3.23 ± 1.51 (−112.09 ± 9.07)	0.46 ± 0.3 (−104.74 ± 8.42)	0.68 ± 0.04 (−88.42 ± 5.71)	10.93 ± 2.73 (−126.61 ± 9.97)	5.25 ± 1.96 (−86.05 ± 23.85)	8.89 ± 1.02 (−69.86 ± 17.22)
Chlorethoxyfos	60.4 ± 3.93 (−61.57 ± 7.25)	5.86 ± 1.05 (−97.95 ± 3.67)	28.35 ± 5.29 (−99.62 ± 4.15)	33.24 ± 24.1 (−86.29 ± 10.57)	37.31 ± 8.41 (−102.25 ± 8.39)	46.17 ± 3.12 (−106.21 ± 5.78)	42.76 ± 2.78 (−109.59 ± 19.45)	46.97 ± 10.59 (−73.32 ± 24.26)
Chlorpyrifos	47.98 ± 3.12 (−49.26 ± 3.39)	1.4 ± 0.46 (−94.86 ± 2.1)	41.15 ± 2.78 (−125.16 ± 6.53)	41.72 ± 15.62 (−112.94 ± 4.14)	36.68 ± 2.48 (−108.05 ± 14.02)	11.91 ± 3.5 (−129.25 ± 5.56)	1.21 ± 0.66 (−68.82 ± 11.78)	2.58 ± 0.83 (−62.49 ± 1.09)
Coumaphos	Inactive	5.51 ± 1.15 (−94.26 ± 3.23)	Inactive	27.07 ± 14.97 (−63.86 ± 15.2)	20.6 ± 18.04 (−22.1 ± 8.11)	22.55 ± 1.52 (−39.59 ± 6.22)	21.06 ± 3.58 (−55.09 ± 9.18)	21.43 ± 5.97 (−37.82 ± 6.23)
Dialifor	41.15 ± 2.78 (−68.77 ± 2.68)	2.69 ± 0.17 (−94.81 ± 1.4)	14.6 ± 0.98 (−103.85 ± 3.74)	25.69 ± 7.15 (−110.07 ± 18.1)	15.74 ± 0 (−95.63 ± 9.9)	15.17 ± 0.98 (−102.32 ± 8.65)	9.74 ± 3.66 (−72.65 ± 10.02)	20.09 ± 4.21 (−64.86 ± 8.68)
EPN	Inactive	2.52 ± 0.47 (−91.48 ± 2.51)	Inactive	Inactive	7.88 ± 11.12 (−16.12 ± 15.74)	Inactive	14.85 ± 3.34 (−40.28 ± 6.85)	26.83 ± 7.94 (−32.65 ± 4.42)
Ethoprop	20.46 ± 6.59 (−84.94 ± 7.67)	2.59 ± 0.17 (−87.77 ± 2.62)	30.27 ± 1.97 (−102.08 ± 10.17)	29.94 ± 26.01 (−71 ± 23.58)	35.25 ± 0 (−85.98 ± 5.72)	39.72 ± 4.56 (−79.82 ± 5.53)	20.34 ± 6.51 (−70.93 ± 11.63)	26.03 ± 19.12 (−54.95 ± 8.8)
Isazofos	10.33 ± 0.69 (−89.49 ± 5.7)	1.15 ± 0.07 (−96.47 ± 0.13)	2.93 ± 0.52 (−111.86 ± 2.56)	6.45 ± 1.79 (−120.97 ± 24.05)	3.14 ± 0 (−98.47 ± 3.32)	0.53 ± 0.03 (−101.96 ± 7.79)	0.11 ± 0.01 (−65.08 ± 3.16)	0.28 ± 0.1 (−58.21 ± 4.65)
Isocarbophos	Inactive	8.21 ± 0.55 (−96.45 ± 3.95)	Inactive	Inactive	41.53 ± 7.47 (−25.66 ± 7.96)	27.76 ± 11.9 (−45.88 ± 8.46)	29.92 ± 8.81 (−55.67 ± 4.1)	23.12 ± 22.23 (−12.32 ± 28.12)
Isoxathion	44.37 ± 0 (−88.55 ± 1.8)	2.11 ± 0.59 (−99.25 ± 1.35)	17.02 ± 1.1 (−104.47 ± 4.63)	26.96 ± 15.29 (−108.22 ± 27.88)	17.74 ± 2.04 (−102.71 ± 1.48)	6.1 ± 3.59 (−127.75 ± 9.7)	0.73 ± 0.24 (−95.65 ± 6.78)	1.68 ± 0.47 (−83.18 ± 15.66)
Leptophos	46.37 ± 5.91 (−61.88 ± 4.89)	2.31 ± 0.15 (−97.46 ± 0.6)	27.99 ± 0 (−85.83 ± 1.88)	54.6 ± 29.18 (−79.45 ± 10.08)	44.57 ± 5.12 (−76.02 ± 9.42)	58.13 ± 3.93 (−41.37 ± 7.01)	36.48 ± 21.08 (−39.42 ± 4.16)	69.03 ± 17.24 (−30.45 ± 4.66)
Parathion	22.75 ± 4.09 (−86.85 ± 6.78)	1.27 ± 0.16 (−93.89 ± 0.75)	11.35 ± 1.44 (−122.26 ± 7.6)	18.07 ± 3.25 (−145.98 ± 15.77)	10.56 ± 1.8 (−105.77 ± 10.92)	6.88 ± 0.79 (−117.21 ± 9.94)	3.9 ± 0.72 (−70.72 ± 9.25)	9.13 ± 2.06 (−64.57 ± 10.9)
Phosalone	Inactive	2.91 ± 0.19 (−93.33 ± 1.43)	Inactive	66.34 ± 14.96 (−53.38 ± 22.17)	50.01 ± 5.75 (−26.69 ± 2.26)	17.11 ± 14.15 (−86.42 ± 12.52)	9.61 ± 9.19 (−92.54 ± 23.57)	10.54 ± 4.6 (−80.05 ± 7.49)
Phoxim	23.43 ± 1.52 (−56.6 ± 4.66)	0.67 ± 0.16 (−84.99 ± 4.79)	20.88 ± 1.36 (−83.75 ± 3.39)	13.26 ± 12.22 (−55.59 ± 12.57)	12.9 ± 2.91 (−71.12 ± 9.11)	3.18 ± 1.08 (−79.26 ± 2.54)	0.33 ± 0.04 (−40.04 ± 9.59)	0.4 ± 0.31 (−40.51 ± 5.34)
Pirimiphos-ethyl	Inactive	12.63 ± 1.45 (−84.22 ± 2.42)	37.23 ± 6.69 (−46.53 ± 2.35)	34.78 ± 13.08 (−70.14 ± 37.03)	34.17 ± 2.23 (−50.07 ± 6.34)	0.8 ± 0.15 (−67.05 ± 3.08)	0.22 ± 0.05 (−47.28 ± 17.04)	0.43 ± 0.06 (−49.9 ± 6.41)
Pyrazophos	49.78 ± 0 (−48.96 ± 11.01)	7.89 ± 0 (−98.21 ± 0.41)	46.17 ± 3.12 (−90.16 ± 2.74)	29.71 ± 12.95 (−97.24 ± 36.89)	46.18 ± 3.13 (−55.34 ± 1.68)	16.38 ± 1.1 (−84.77 ± 1.6)	2.46 ± 0.68 (−85.05 ± 15.3)	4.46 ± 0.51 (−79.77 ± 7.95)
Quinalphos	55.86 ± 0 (−32.59 ± 1.41)	1.77 ± 0.2 (−94.19 ± 1.06)	46.37 ± 5.91 (−109.17 ± 9.49)	29.37 ± 14.36 (−90.48 ± 6.5)	46.18 ± 3.13 (−84.31 ± 2.26)	7.48 ± 4.34 (−111.89 ± 8.58)	1.64 ± 0.2 (−81.26 ± 17.15)	2.94 ± 0.53 (−80.23 ± 8.04)
Tebupirimfos	46.17 ± 3.12 (−53.09 ± 5.95)	4.29 ± 0.59 (−93.85 ± 0.95)	20.07 ± 3.74 (−98.46 ± 4.72)	28.24 ± 16 (−99.19 ± 14.9)	24.16 ± 3.32 (−93.89 ± 3.28)	9.97 ± 1.14 (−121.54 ± 0.85)	2.08 ± 0.37 (−86.44 ± 20.27)	3.7 ± 0.67 (−78.68 ± 13.94)
Terbufos	Inactive	4.27 ± 0.27 (−88.06 ± 0.57)	Inactive	2.19 ± 2.53 (−37.43 ± 11.78)	35.4 ± 4.07 (−86.04 ± 5.48)	2.31 ± 0.15 (−39.73 ± 8.54)	1.83 ± 1.13 (−43.48 ± 3.61)	1.36 ± 0.23 (−58.45 ± 5.48)
Triazophos	50 ± 5.74 (−40.48 ± 3.78)	3.02 ± 0.19 (−98.33 ± 0.85)	36.68 ± 2.48 (−105.28 ± 8.71)	31.25 ± 23.78 (−94.48 ± 5.77)	33.25 ± 7.5 (−52.01 ± 12.34)	2.44 ± 0.61 (−86.48 ± 5.5)	0.91 ± 0.38 (−61.35 ± 6.28)	14.03 ± 0 (−43.50 ± 0)
Tribufos	35.26 ± 12.58 (−42.24 ± 2.97)	3.66 ± 0.24 (−92.54 ± 0.51)	15.3 ± 2.6 (−70.4 ± 6.71)	12.16 ± 12.31 (−31.22 ± 7.71)	12.05 ± 0.79 (−103.4 ± 2.65)	39.81 ± 6.45 (−50.65 ± 5.03)	31.41 ± 0 (−68.44 ± 0)	4.36 ± 1.09 (−56.29 ± 0.3)

Note: Each value of potency (IC_{50}, μM) and efficacy (percent of positive control, expressed in parentheses) is the mean ± standard deviation (SD) of the results from three experiments. SH-SY5Y spheroids (24 h), SH-SY5Y spheroids (48 h), neural stem cell spheroids (24 h), or neural stem cell spheroids (48 h): AChE assays were performed after these cells were cultured in spheroid formation for 24 h or 48 h. IC_{50}, concentration of half-maximal inhibition.

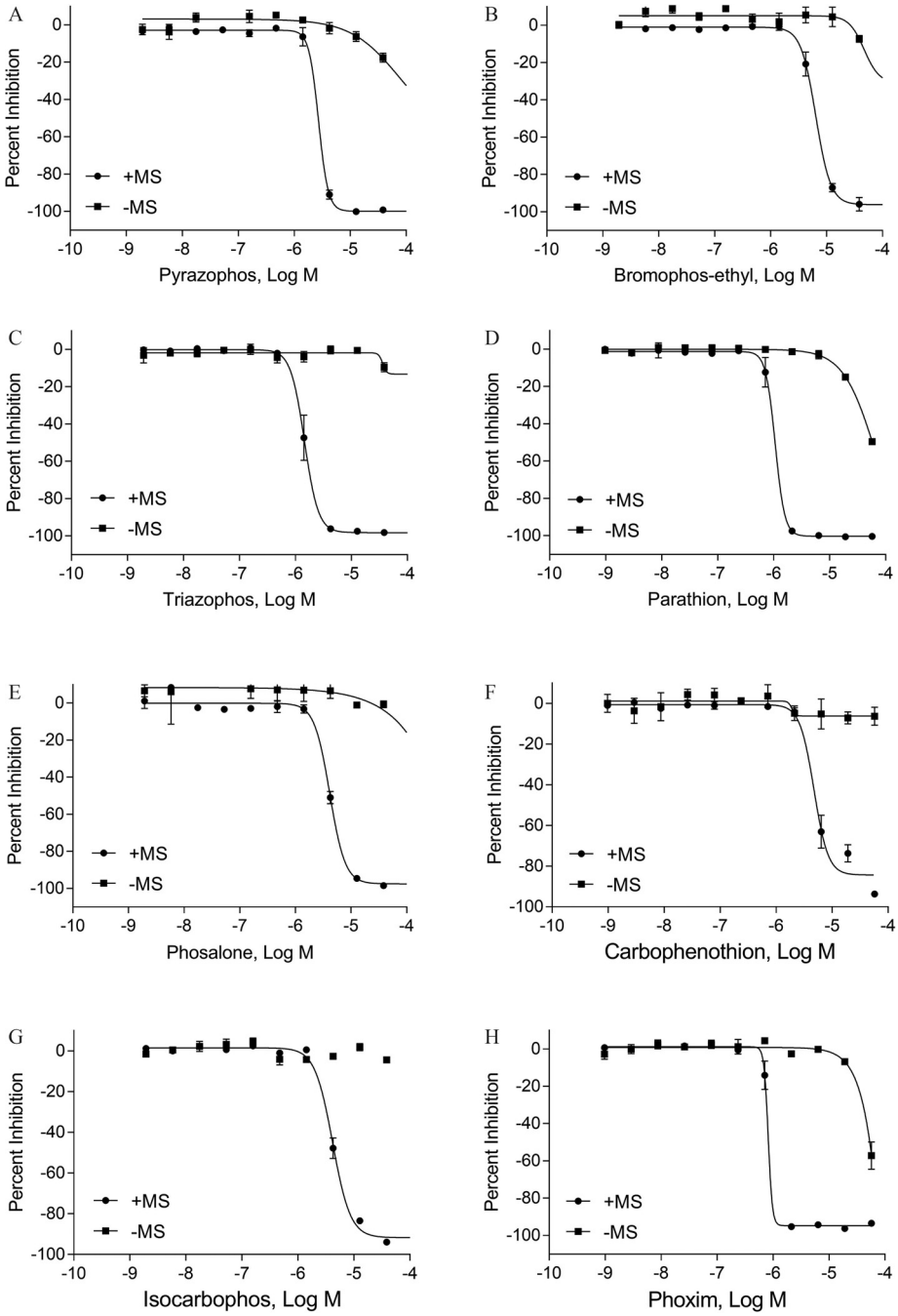

Figure 3. Concentration response curves of representative parent compounds in AChE assay with or without human liver microsomes (MS). (A) pyrazophos; (B) phosalone; (C) triazophos; (D) parathion; (E) bromophos-ethyl; (F) carbophenothion; (G) isocarbophos; and (H) Phoxim. Each value represents the mean ± standard deviation (SD) of three independent experiments.

significantly higher in spheroid in comparison with monolayer cell cultures (Figure S4E and S4F; Excel Table S10). There was no difference in gene expression of cyp3a4 and cyp2d6 between monolayer and spheroid for SH-SY5Y cells (Figure S4E and S4F; Excel Table S10). No cyp1a2 and cyp2b6 gene expression were detected in both neural stem cells and SH-SY5Y cells in either monolayer or spheroid format.

Characterizations of Reversible and Irreversible AChE Inhibitors

To study the mode of compound action, the reversibility of AChE inhibition by these compounds was investigated. For the 111 compounds, 95 were previously reported as AChE inhibitors, whereas 16 compounds were previously not reported as AChE inhibitors. Among the 111 compounds identified from the primary HTS, 60 employ at least one reactive functionality that can form a covalent bond with the Serine residue (Ser203) in the AChE active site (Fukuto 1990; Johnson et al. 2011; Venkatasubban et al. 2018). Within this group, we identified one alkylated pyridine (Johnson et al. 2011), 37 OPs (Fukuto 1990), and 22 carbamates (Venkatasubban et al. 2018). The rest of the compounds without any Serine reactive group may inhibit the enzymatic activity of AChE through a reversible mechanism. We then confirmed the reversibility of these AChE inhibitors by comparing their IC_{50} or efficacy values at different time points. The

compounds were incubated with AChE for 5, 10, and 60 min, and the IC_{50} values at different time points were calculated (Excel Table S11). For the 95 known inhibitors, 41 reversible inhibitors were found in a time-independent manner, and 40 irreversible inhibitors were found to be time dependent, which was consistent with literature reports (Colović et al. 2013; Pohanka 2011). There were 14 compounds that did not show inhibitory activity against AChE in the three time points. In the current study, the irreversibility of some AChE inhibitors used as pesticides, such as chlorpyrifos-oxon, diazinon, and dialifor, were confirmed, whereas the reversibility of some AChE inhibitors, such as tacrine hydrochloride, donepezil, and rivastigmine, which are used as drugs for treating AD, were also confirmed. Chlorpyrifos-oxon and ambenonium chloride were the most potent irreversible and reversible AChE inhibitor, respectively. The carbamate compounds have been reported to be both reversible and irreversible in AChE inhibition (Fukuto 1990). In our study, the carbamate compounds, such as aldicarb and carbaryl, showed no IC_{50} differences between 5 and 10 min but did show a significant IC_{50} difference at 60 min. All 16 previously not identified AChE inhibitors, including orlistat and tilorone, appeared to be reversible AChE inhibitors.

Molecular Docking Study

To explore the interactions between AChE and the inhibitors, molecular docking was employed to study the binding mode of these 111 AChE inhibitors plus 2,3-Dihydro-2,2-dimethyl-7-benzofuranol as an inactive control. The docking results showed that all the AChE inhibitors were predicted to bind the active sites of the AChE, except endosulfan I and triethyl phosphite (Table S2). The primary qHTS results indicated that four pairs of compounds (aldicarb/aldicarb sulfoxide, chlorpyrifos/chlorpyrifos oxon, diazinon/diazoxon, parathion/paraoxon) had large potency differences in AChE inhibition. Then docking was used to compare the binding modes of these four pairs. The results showed that aldicarb and aldicarb sulfoxide exhibited similar binding modes in the active site of AChE (Figure 4A). Specifically, the carbamoyl oxime fragment of both aldicarb and aldicarb sulfoxide occupied the same hydrophobic pocket formed by Tyr72, Trp286, Tyr341, and Phe338. Because the length of aldicarb sulfoxide was slightly longer than that of aldicarb, it can fit more deeply into the active site of AChE, bringing the sulfoxide oxygen atom within H-bonding distance of the active site residue Ser203. In addition, the sulfoxide oxygen atom was also located near His447, Gly121, and Gly122, which all contain H-bond donors that could interact with the oxygen atom of the sulfoxide atom. These additional interactions between aldicarb sulfoxide and AChE agreed with the result that aldicarb sulfoxide was 15-fold more potent than aldicarb (0.61 μM vs. 8.89 μM). No binding mode differences were found between the other three pairs. In addition, 2,3-Dihydro-2,2-dimethyl-7-benzofuranol, which was inactive in the AChE inhibition assay, was also predicted to dock into the active site of AChE. As shown in Figure 4B, this compound preferred to stay at the entrance of the active site instead of binding into the acetylcholine binding pocket, which may explain its inactivity.

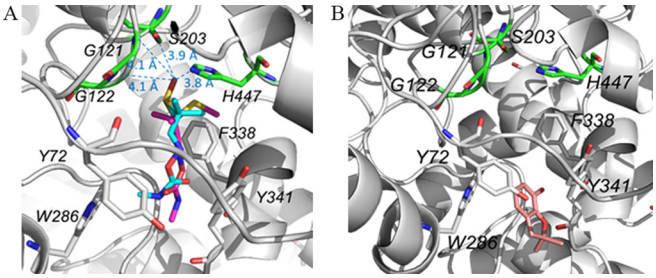

Figure 4. Molecular docking result of aldicarb (carbon atoms in magenta) and aldicarb sulfoxide (carbon atoms in cyan) (A) and inactive hit 2, 3-dihydro-2, 2-dimethyl-7-benzofuranol (B) in the active site of AChE (gray, PDB: 4EY7). Key residues of AChE that interact the sulfoxide oxygen atom were shown in stick. The residues that potentially interact with aldicarb sulfoxide but not aldicarb were highlighted in green. Note: PDB, Protein Data Bank.

Discussion

In this study, we used multiple qHTS assays to screen and profile the Tox21 10K compound library for AChE inhibition activity. Cell-based assays using SH-SY5Y cells and enzyme-based assays using recombinant human AChE protein with or without human liver microsomes addition were employed to understand the biological activity of these compounds. SAR analysis was used to characterize the structural features of the AChE inhibitors identified. This screening approach, combined with secondary follow-up studies including the use of neural stem cells, spheroids, experiments to test reaction reversibility, and molecular docking analyses, enabled efficient screening of large chemical libraries to identify potential novel AChE inhibitors.

Approximately 2.25% (187 compounds) of the compounds in the Tox21 10K library inhibited AChE activity (Figure 1). Based on potency and efficacy, 111 compounds were selected for testing in additional cell models along with molecular docking studies. Of the 111 compounds, 100 compounds were active in both cell-based and enzyme-based assays, and 19 compounds were potent AChE inhibitors with $IC_{50} < 1$ μM. Among these compounds, some are known AChE inhibitors approved for AD treatment, such as donepezil and rivastigmine (Kumar et al. 2018), whereas others are widely used pesticides, such as aldicarb, carbaryl, and chlorpyrifos. In this study, we identified several potentially novel AChE inhibitors, most of which are clinically used drugs. For example, orlistat, a natural inhibitor of pancreatic lipases used for treating obesity (Heck et al. 2000), was identified as a potent AChE inhibitor. Obesity is regarded as one of risk factors for AD (Alford et al. 2018). Tilorone, an active interferon inducer used for treating virus infection (Krueger and Mayer 1970), was also shown to inhibit AChE. Therefore, orlistat and tilorone may be considered as potential drugs that can be repurposed for treating AD. Other apparently novel AChE inhibitors, such as amisulpride, bromopride, ecopipam, and trimethobenzamide, are dopamine receptor antagonists that can be used for treatment of neurological disorders (Chipkin et al. 1988; Pani and Gessa 2002; Smith et al. 2012; Tonini et al. 2004). On the other hand, orlistat and tilorone are known to have side effects in humans, including nausea and vomiting, which may be due to AChE inhibition (Kaufman et al. 1971; Lean et al. 2014). Recently, polyoxometalate compounds were also shown to be potent AChE inhibitors (Čolović et al. 2017; Jamshed Iqbal 2013). Therefore, identifying these potentially novel AChE inhibitors is important for repurposing existing drugs or for identifying adverse side effects among a range of compounds with relevance to human health and safety.

The Tox21 10K compound library was grouped into 1,014 clusters based on structure similarity, more than 30 of which were significantly enriched with active AChE inhibitors. Several structural motifs emerged in the enriched clusters, and these may constitute pharmacophores or toxicophores for AChE inhibitory effect. The significantly enriched cluster ($p = 4.57 \times 10^{-11}$) contained 21 compounds, which belong to carbamates. Another enriched cluster was a group of OP compounds that were more active in the cell-based AChE inhibition assay ($p < 0.01$) than in the enzyme-based AChE inhibition assay ($p > 0.01$). Carbamates and OPs are two major groups of known AChE inhibitors (Fukuto 1990). In addition, one enriched cluster found to be

active contained acridines, which have been shown to be effective as inhibitors of acetylcholinesterase in pharmacotherapy of AD (Arya et al. 2015). It is interesting to note that dyes such as basic blue and the fluorescent rhodamine-family dyes also had inhibitory effect on AChE. A group of alkaloids were also enriched with compounds that were active in our assay ($p < 0.01$). Two potentially novel AChE inhibitors, moxisylyte hydrochloride and tilorone, belonged to one of the enriched clusters.

Some OPs that showed no or weak AChE inhibition, needed biotransformation to be effective AChE inhibitors (Sultatos 1994). In our study, seven parental OPs, including carbophenothion, coumaphos, EPN, isocarbophos, phosalone, pirimiphos-ethyl, and terbufos, did not show effects in our AChE inhibition assays. In the presence of microsomes, these seven compounds were potent AChE inhibitors with IC_{50}s of 2.52 to 12.63 μM. There are 18 additional compounds that were more potent with the addition of microsomes (IC_{50} value difference ≥3-fold between assays with and without microsomes). Human CYPs, such as CYP2B6 and CYP3A4, are mainly responsible for the biotransformation of certain pesticides (Abass et al. 2011). The microsomes used in our study contain the nine most common CYPs, including CYP3A4 and CYP2B6 (Table S4). The thio starting compounds can be transformed to their oxo analogs, which are more potent AChE inhibitors in comparison with the parent compound (Colović et al. 2010; Krstić et al. 2007; Čolović 2011).

In addition to metabolic activation, there is also metabolic degradation that can result in detoxified metabolites (Ma and Chambers 1994). Understanding the potential risk of chemicals to humans is likely dependent on the balance between the activating and detoxifying processes. Some of the parent OPs were not activated by human microsomes, such as diazinon, dimethoate, malathion, and pirimiphos-methyl, consistent with our previous data (Li et al. 2019). For example, malathion can be metabolized by CYPs to malaoxon, a potent AChE inhibitor, whereas it can also be rapidly degraded by carboxylesterases (Buratti et al. 2005). This degradation may be the reason why malathion was not identified to inhibit AChE, but its metabolite, malaoxon, showed potent inhibition of AChE with IC_{50} of 1.46 μM. Moreover, serum albumin may play a role in the detoxication of OPs and carbamate pesticides by hydrolyzing the AChE inhibitors (Li et al. 2008; Sogorb and Vilanova 2010). Two carbamates, benfuracarb and carbosulfan, were more potent AChE inhibitors after metabolic activation. An interesting finding was that several compounds that included phosalone were more potent in spheroids than in the monolayer cell culture (Table 2). This potency difference may be due to the difference in the CYP expression level and activities in these monolayer and spheroid cultures. The activities of some CYPs, including CYP1A and CYP3A4, were shown to be enhanced in 3D hepatocyte models (Shoemaker and Vukasinovic 2017). CYP enzymes, such as CYP1A, CYP2D6 and CYP2E1, are expressed in SH-SY5Y cells (Fernandez-Abascal et al. 2018; Mann and Tyndale 2010). Compared with SH-SY5Y cells, some compounds like bromophos-ethyl, phosalone, and quinalphos were more potent AChE inhibitors in neuronal stem cells. This greater potency may be caused by the difference in CYP activities between neuronal stem cells and SH-SY5Y cells. Our results showed that spheroid neuronal stem cells had higher CYP3A4 and CYP2D6 activities and gene expression than the monolayer cell culture of neuronal stem cells. However, the CYP1A2 and CYP2B6 could not be detected in either neuronal stem cells or SH-SY5Y cells using P450-Glo assays and qPCR analysis.

There are irreversible and reversible AChE inhibitors based on their mode of action. OP compounds are known to be irreversible AChE inhibitors that can form a strong covalent bond with the Ser203 of the catalytic triad in the AChE active site, whereas carbamates are reversible AChE inhibitors that form a weak covalent bond (Colović et al. 2013). Of the 111 compounds, 37 OP compounds were shown to inhibit AChE irreversibly. Twenty-two carbamates in our study showed dual mechanism (reversible and irreversible) in inhibiting AChE. The inhibition by carbamates has been shown to be "pseudoirreversible" or "slowly reversible," because the hydrolysis of the carbamoyl enzyme is slow (Darvesh et al. 2008). This hydrolysis process is also influenced by the size of the carbamoyl groups (Venkatasubban et al. 2018). Sixteen drugs were identified as potentially novel, reversible AChE inhibitors that could cause adverse effects. In addition, these drugs have the potential to be developed for the treatment of neurological diseases.

Molecular docking is a useful tool for exploring the interactions between AChE and its inhibitors. We found that aldicarb and its metabolite inhibited AChE at different potencies. Molecular docking showed that the S = O group (not the reactive C = O groups) in aldicarb sulfoxide can form additional interactions with residues in the active site, which may contribute to its improved IC_{50} value. This type of contribution is not relevant for the other three pairs (chlorpyrifos/chlorpyrifos-oxon, diazinon/diazoxon, parathion/paraoxon) that showed differential potencies in AChE inhibition, which may be contributed to the change of P = S to P = O, instead of additional interactions with the active site residues.

Conclusions

Using tiered qHTS assays, we profiled more than 8,300 compounds with relevance to human health for their ability to inhibit AChE. Many AChE inhibitors can act as pesticides or drugs with either toxicological effects or pharmaceutical applications (Colović et al. 2013). The combination of cell-based and enzyme-based assays in a robust screening platform allowed us to identify AChE inhibitors efficiently and quickly. From this study, several key chemical structural motifs were identified to be highly associated with AChE inhibition. These AChE inhibitors were shown to bind to the active site of AChE using molecular docking. Several potentially novel AChE inhibitors identified from our study may have the potential to be repurposed as therapies for neurological diseases, such as AD, or to cause toxicity, both of which are important regarding human health outcomes. In addition, the pharmacological application of AChE inhibitors for the treatment of other neurological disorders, such as Parkinson's disease, dementia, myasthenia gravis, and Lewy bodies, remains to be elucidated. The potentially novel AChE inhibitors identified from our study can be further tested *in vivo* to provide enhanced understanding of the pharmacokinetic and toxicokinetic properties of the compounds. The use of tiered qHTS assays in combination with conformational and mechanistic follow-up studies allowed us to evaluate thousands of compounds for their inhibitory effects on AChE. The large data set generated from this study is also valuable in developing computational models that can be used to predict new AChE inhibitors.

Acknowledgments

This study was supported in part by the Intramural Research Program of the NCATS and Interagency Agreement IAA #NTR 12003 from the National Institute of Environmental Health Sciences Division of the NTP to the NCATS, National Institutes of Health (NIH). The authors thank Z. Itkin and P. Shinn for compound management, C. Lynch for technique advice of RT-PCR experiment, and A. Li for editing the manuscript.

The views expressed in this paper are those of the authors and do not necessarily reflect the statements, opinions, views, conclusions, or policies of the NCATS, the NIH, or the U.S. Food

and Drug Administration. Mention of trade names or commercial products does not constitute endorsement or recommendation for use.

References

Abass K, Turpeinen M, Rautio A, Hakkola J, Pelkonen O. 2011. Metabolism of pesticides by human cytochrome P450 enzymes in vitro - a survey. In: *Insecticides - Advances in Integrated Pest Management* Perveen FK, ed. InTech, 165–194, https://doi.org/10.13140/2.1.3501.5689.

Alford S, Patel D, Perakakis N, Mantzoros CS. 2018. Obesity as a risk factor for Alzheimer's disease: weighing the evidence. Obes Rev 19(2):269–280, PMID: 29024348, https://doi.org/10.1111/obr.12629.

Almasieh M, MacIntyre JN, Pouliot M, Casanova C, Vaucher E, Kelly ME, et al. 2013. Acetylcholinesterase inhibition promotes retinal vasoprotection and increases ocular blood flow in experimental glaucoma. Invest Ophthalmol Vis Sci 54(5):3171–3183, PMID: 23599333, https://doi.org/10.1167/iovs.12-11481.

Arya S, Kumar A, Kumar N, Roy P, Sondhi SM. 2015. Synthesis and anticancer activity evaluation of some acridine derivatives. Med Chem Res 24(5):1942–1951, https://doi.org/10.1007/s00044-014-1268-6.

Attene-Ramos MS, Miller N, Huang R, Michael S, Itkin M, Kavlock RJ, et al. 2013. The Tox21 robotic platform for the assessment of environmental chemicals–from vision to reality. Drug Discov Today 18(15–16):716–723, PMID: 23732176, https://doi.org/10.1016/j.drudis.2013.05.015.

Battisti V, Schetinger MRC, Maders LDK, Santos KF, Bagatini MD, Correa MC, et al. 2009. Changes in acetylcholinesterase (ache) activity in lymphocytes and whole blood in acute lymphoblastic leukemia patients. Clin Chim Acta 402(1–2):114–118, PMID: 19185568, https://doi.org/10.1016/j.cca.2008.12.030.

Bowes J, Brown AJ, Hamon J, Jarolimek W, Sridhar A, Waldron G, et al. 2012. Reducing safety-related drug attrition: the use of in vitro pharmacological profiling. Nat Rev Drug Discov 11(12):909–922, PMID: 23197038, https://doi.org/10.1038/nrd3845.

Buratti FM, D'Aniello A, Volpe MT, Meneguz A, Testai E. 2005. Malathion bioactivation in the human liver: the contribution of different cytochrome p450 isoforms. Drug Metab Dispos 33(3):295–302, PMID: 15557345, https://doi.org/10.1124/dmd.104.001693.

Castillo-González AC, Nieto-Cerón S, Pelegrín-Hernández JP, Montenegro MF, Noguera JA, López-Moreno MF, et al. 2015. Dysregulated cholinergic network as a novel biomarker of poor prognostic in patients with head and neck squamous cell carcinoma. BMC Cancer 15(1), PMID: 25956553, https://doi.org/10.1186/s12885-015-1402-y.

Chipkin RE, Iorio LC, Coffin VL, McQuade RD, Berger JG, Barnett A. 1988. Pharmacological profile of SCH39166: a dopamine D1 selective benzonaphthazepine with potential antipsychotic activity. J Pharmacol Exp Ther 247(3):1093–1102, PMID: 2905002.

Colović MB, Krstić DZ, Lazarević-Pašti TD, Bondžić AM, Vasić VM. 2013. Acetylcholinesterase inhibitors: pharmacology and toxicology. Curr Neuropharmacol 11(3):315–335, PMID: 24179466, https://doi.org/10.2174/1570159X11311030006.

Colović M, Krstić D, Petrović S, Leskovac A, Joksić G, Savić J, et al. 2010. Toxic effects of diazinon and its photodegradation products. Toxicol Lett 193(1):9–18, PMID: 19948211, https://doi.org/10.1016/j.toxlet.2009.11.022.

Čolović MB, Krstić DZ, Ušćumlić GS, Vasić VM. 2011. Single and simultaneous exposure of acetylcholinesterase to diazinon, chlorpyrifos and their photodegradation products. Pestic Biochem Physiol 100(1):16–22, https://doi.org/10.1016/j.pestbp.2011.01.010.

Čolović MB, Medić B, Ćetković M, Kravić Stevović T, Stojanović M, Ayass WW, et al. 2017. Toxicity evaluation of two polyoxotungstates with anti-acetylcholinesterase activity. Toxicol Appl Pharmacol 333:68–75, PMID: 28830837, https://doi.org/10.1016/j.taap.2017.08.010.

Darvesh S, Darvesh KV, McDonald RS, Mataija D, Walsh R, Mothana S, et al. 2008. Carbamates with differential mechanism of inhibition toward acetylcholinesterase and butyrylcholinesterase. J Med Chem 51(14):4200–4212, PMID: 18570368, https://doi.org/10.1021/jm8002075.

Du A, Xie J, Guo K, Yang L, Wan Y, OuYang Q, et al. 2015. A novel role for synaptic acetylcholinesterase as an apoptotic deoxyribonuclease. Cell Discov 1:15002, PMID: 27462404, https://doi.org/10.1038/celldisc.2015.2.

Farahat FM, Ellison CA, Bonner MR, McGarrigle BP, Crane AL, Fenske RA, et al. 2011. Biomarkers of chlorpyrifos exposure and effect in Egyptian cotton field workers. Environ Health Perspect 119(6):801–806, PMID: 21224175, https://doi.org/10.1289/ehp.1002873.

Fernandez-Abascal J, Ripullone M, Valeri A, Leone C, Valoti M. 2018. β-naphtoflavone and ethanol induce cytochrome P450 and protect towards MPP^+ toxicity in human neuroblastoma SH-SY5Y cells. Int J Mol Sci 19(11):3369, PMID: 30373287, https://doi.org/10.3390/ijms19113369.

Fukuto TR. 1990. Mechanism of action of organophosphorus and carbamate insecticides. Environ Health Perspect 87:245–254, PMID: 2176588, https://doi.org/10.1289/ehp.9087245.

Guvench O, MacKerell AD Jr. 2009. Computational fragment-based binding site identification by ligand competitive saturation. PLoS Comput Biol 5(7):e1000435, PMID: 19593374, https://doi.org/10.1371/journal.pcbi.1000435.

Heck AM, Yanovski JA, Calis KA. 2000. Orlistat, a new lipase inhibitor for the management of obesity. Pharmacotherapy 20(3):270–279, PMID: 10730683, https://doi.org/10.1592/phco.20.4.270.34882.

Hess B, Kutzner C, van der Spoel D, Lindahl E. 2008. GROMACS 4: algorithms for highly efficient, load-balanced, and scalable molecular simulation. J Chem Theory Comput 4(3):435–447, PMID: 26620784, https://doi.org/10.1021/ct700301q.

Huang J, Rauscher S, Nawrocki G, Ran T, Feig M, de Groot BL, Grubmuller H, Mackerell AD. 2017. CHARMM36m: an improved force field for folded and intrinsically disordered proteins. Nature Methods 14:71–73, http://mackerell.umaryland.edu/charmm_ff.shtml.

Huang R. 2016. A quantitative high-throughput screening data analysis pipeline for activity profiling. Methods Mol Biol 1473:111–122, PMID: 27518629, https://doi.org/10.1007/978-1-4939-6346-1_12.

Huang R, Xia M, Cho MH, Sakamuru S, Shinn P, Houck KA, et al. 2011. Chemical genomics profiling of environmental chemical modulation of human nuclear receptors. Environ Health Perspect 119(8):1142–1148, PMID: 21543282, https://doi.org/10.1289/ehp.1002952.

Huang R, Xia M, Sakamuru S, Zhao J, Shahane SA, Attene-Ramos M, et al. 2016. Modelling the Tox21 10 K chemical profiles for in vivo toxicity prediction and mechanism characterization. Nat Commun 7:10425, PMID: 26811972, https://doi.org/10.1038/ncomms10425.

Inglese J, Auld DS, Jadhav A, Johnson RL, Simeonov A, Yasgar A, et al. 2006. Quantitative high-throughput screening: a titration-based approach that efficiently identifies biological activities in large chemical libraries. Proc Natl Acad Sci USA 103(31):11473–11478, PMID: 16864780, https://doi.org/10.1073/pnas.0604348103.

Iqbal J, Barsukova-Stuckart M, Ibrahim M, Ali SU, Khan AA, Kortz U. 2013. Polyoxometalates as potent inhibitors for acetyl and butyrylcholinesterases and as potential drugs for the treatment of Alzheimer's disease. Med Chem Res 22(3):1224–1228, https://doi.org/10.1007/s00044-012-0125-8.

Johnson CM, Linsky TW, Yoon DW, Person MD, Fast W. 2011. Discovery of halopyridines as quiescent affinity labels: inactivation of dimethylarginine dimethylaminohydrolase. J Am Chem Soc 133(5):1553–1562, PMID: 21222447, https://doi.org/10.1021/ja109207m.

Kaufman HE, Centifanto YM, Ellison ED, Brown DC. 1971. Tilorone hydrochloride: human toxicity and interferon stimulation. Proc Soc Exp Biol Med 137(1):357–360, PMID: 5581674, https://doi.org/10.3181/00379727-137-35576.

Kohonen T. 2006. Self-organizing neural projections. Neural Netw 19(6–7):723–733, PMID: 16774731, https://doi.org/10.1016/j.neunet.2006.05.001.

Krewski D, Andersen ME, Mantus E, Zeise L. 2009. Toxicity testing in the 21st century: implications for human health risk assessment. Risk Anal 29(4):474–479, PMID: 19144067, https://doi.org/10.1111/j.1539-6924.2008.01150.x.

Krstić D, Colović M, Krinulović K, Djurić D, Vasić V. 2007. Inhibition of AChE by single and simultaneous exposure to malathion and its degradation products. Gen Physiol Biophys 26:247–253, PMID: 18281741.

Krueger RE, Mayer GD. 1970. Tilorone hydrochloride: an orally active antiviral agent. Science 169(3951):1213–1214, PMID: 4317923, https://doi.org/10.1126/science.169.3951.1213.

Kumar K, Kumar A, Keegan RM, Deshmukh R. 2018. Recent advances in the neurobiology and neuropharmacology of Alzheimer's disease. Biomed Pharmacother 98:297–307, PMID: 29274586, https://doi.org/10.1016/j.biopha.2017.12.053.

Lakkaraju SK, Yu W, Raman EP, Hershfeld AV, Fang L, Deshpande DA, et al. 2015. Mapping functional group free energy patterns at protein occluded sites: nuclear receptors and G-protein coupled receptors. J Chem Inf Model 55(3):700–708, PMID: 25692383, https://doi.org/10.1021/ci500729k.

Lean ME, Carraro R, Finer N, Hartvig H, Lindegaard ML, Rössner S, et al. 2014. Tolerability of nausea and vomiting and associations with weight loss in a randomized trial of liraglutide in obese, non-diabetic adults. Int J Obes 38(5):689–697, PMID: 23942319, https://doi.org/10.1038/ijo.2013.149.

Li SZ, Huang RL, Solomon S, Liu YT, Zhao B, Santillo MF, et al. 2017. Identification of acetylcholinesterase inhibitors using homogenous cell-based assays in quantitative high-throughput screening platforms. Biotechnol J 12(5):1600715, PMID: 28294544, https://doi.org/10.1002/biot.201600715.

Li B, Nachon F, Froment MT, Verdier L, Debouzy JC, Brasme B, et al. 2008. Binding and hydrolysis of soman by human serum albumin. Chem Res Toxicol 21(2):421–431, PMID: 18163544, https://doi.org/10.1021/tx700339m.

Li SZ, Zhao JH, Huang RL, Santillo MF, Houck KA, Xia MH. 2019. Use of high-throughput enzyme-based assay with xenobiotic metabolic capability to evaluate the inhibition of acetylcholinesterase activity by organophosphorous pesticides. Toxicol In Vitro 56:93–100, PMID: 30625376, https://doi.org/10.1016/j.tiv.2019.01.002.

Ma T, Chambers JE. 1994. Kinetic parameters of desulfuration and dearylation of parathion and chlorpyrifos by rat liver microsomes. Food Chem Toxicol 32(8):763–767, PMID: 7520881, https://doi.org/10.1016/s0278-6915(09)80009-4.
Mann A, Tyndale RF. 2010. Cytochrome P450 2D6 enzyme neuroprotects against 1-methyl-4-phenylpyridinium toxicity in SH-SY5Y neuronal cells. Eur J Neurosci 31(7):1185–1193, PMID: 20345925, https://doi.org/10.1111/j.1460-9568.2010.07142.x.
Martínez-Moreno P, Nieto-Cerón S, Torres-Lanzas J, Ruiz-Espejo F, Tovar-Zapata I, Martínez-Hernández P, et al. 2006. Cholinesterase activity of human lung tumours varies according to their histological classification. Carcinogenesis 27(3):429–436, PMID: 16272577, https://doi.org/10.1093/carcin/bgi250.
Massoulié J, Pezzementi L, Bon S, Krejci E, Vallette FM. 1993. Molecular and cellular biology of cholinesterases. Prog Neurobiol 41(1):31–91, PMID: 8321908, https://doi.org/10.1016/0301-0082(93)90040-y.
Montenegro MF, Ruiz-Espejo F, Campoy FJ, Muñoz-Delgado E, Páez de la Cadena M, Cabezas-Herrera J, et al. 2006. Acetyl- and butyrylcholinesterase activities decrease in human colon adenocarcinoma. J Mol Neurosci 30(1–2):51–54, PMID: 17192624, https://doi.org/10.1385/JMN:30:1:51.
Mukherjee PK, Kumar V, Mal M, Houghton PJ. 2007. Acetylcholinesterase inhibitors from plants. Phytomedicine 14(4):289–300, PMID: 17346955, https://doi.org/10.1016/j.phymed.2007.02.002.
Neria E, Fischer S, Karplus M. 1996. Simulation of activation free energies in molecular systems. J Chem Phys 105(5):1902–1921, https://doi.org/10.1063/1.472061.
Ohbe H, Jo T, Matsui H, Fushimi K, Yasunaga H. 2018. Cholinergic crisis caused by cholinesterase inhibitors: a retrospective nationwide database study. J Med Toxicol 14(3):237–241, PMID: 29907949, https://doi.org/10.1007/s13181-018-0669-1.
Pani L, Gessa GL. 2002. The substituted benzamides and their clinical potential on dysthymia and on the negative symptoms of schizophrenia. Mol Psychiatry 7(3):247–253, PMID: 11920152, https://doi.org/10.1038/sj.mp.4001040.
Pohanka M. 2011. Cholinesterases, a target of pharmacology and toxicology. Biomed Pap Med Fac Univ Palacky Olomouc Czech Repub 155(3):219–229, PMID: 22286807, https://doi.org/10.5507/bp.2011.036.
Raman EP, Yu W, Lakkaraju SK, MacKerell AD Jr. 2013. Inclusion of multiple fragment types in the site identification by ligand competitive saturation (SILCS) approach. J Chem Inf Model 53(12):3384–3398, PMID: 24245913, https://doi.org/10.1021/ci4005628.
Richard AM, Huang R, Waidyanatha S, Shinn P, Collins BJ, Thillainadarajah I, et al. 2020. The Tox21 10K compound library: collaborative chemistry advancing toxicology. Chem Res Toxicol 34(2):189–216, PMID: 33140634, https://doi.org/10.1021/acs.chemrestox.0c00264.
Shoemaker JT, Vukasinovic J. 2017. Cytochrome P450 enzyme activity is enhanced in hepatocytes grown using a perfused 3D cell culture drug screening system. Cancer Res 77(suppl 13):4080, https://doi.org/10.1158/1538-7445.AM2017-4080.
Smith HS, Cox LR, Smith BR. 2012. Dopamine receptor antagonists. Ann Palliat Med 1(2):137–142, PMID: 25841474, https://doi.org/10.3978/j.issn.2224-5820.2012.07.09.
Sogorb MA, Vilanova E. 2010. Serum albumins and detoxication of anticholinesterase agents. Chem Biol Interact 187(1–3):325–329, PMID: 20211614, https://doi.org/10.1016/j.cbi.2010.03.001.
Soreq H, Seidman S. 2001. Acetylcholinesterase–new roles for an old actor. Nat Rev Neurosci 2(4):294–302, PMID: 11283752, https://doi.org/10.1038/35067589.
Suarez-Lopez JR, Jacobs DR Jr, Himes JH, Alexander BH. 2013. Acetylcholinesterase activity, cohabitation with floricultural workers, and blood pressure in Ecuadorian children. Environ Health Perspect 121(5):619–624, PMID: 23359481, https://doi.org/10.1289/ehp.1205431.
Sultatos LG. 1994. Mammalian toxicology of organophosphorus pesticides. J Toxicol Environ Health 43(3):271–289, PMID: 7966438, https://doi.org/10.1080/15287399409531921.
Thomas RS, Paules RS, Simeonov A, Fitzpatrick SC, Crofton KM, Casey WM, et al. 2018. The US Federal Tox21 Program: a strategic and operational plan for continued leadership. ALTEX 35(2):163–168, PMID: 29529324, https://doi.org/10.14573/altex.1803011.
Tice RR, Austin CP, Kavlock RJ, Bucher JR. 2013. Improving the human hazard characterization of chemicals: a Tox21 update. Environ Health Perspect 121(7):756–765, PMID: 23603828, https://doi.org/10.1289/ehp.1205784.
Tonini M, Cipollina L, Poluzzi E, Crema F, Corazza GR, De Ponti F. 2004. Review article: clinical implications of enteric and central D2 receptor blockade by antidopaminergic gastrointestinal prokinetics. Aliment Pharmacol Ther 19(4):379–390, PMID: 14871277, https://doi.org/10.1111/j.1365-2036.2004.01867.x.
Ustach VD, Lakkaraju SK, Jo S, Yu W, Jiang W, MacKerell AD Jr. 2019. Optimization and evaluation of site-identification by ligand competitive saturation (SILCS) as a tool for target-based ligand optimization. J Chem Inf Model 59(6):3018–3035, PMID: 31034213, https://doi.org/10.1021/acs.jcim.9b00210.
Vanommeslaeghe K, Hatcher E, Acharya C, Kundu S, Zhong S, Shim J, et al. 2010. CHARMM general force field: a force field for drug-like molecules compatible with the CHARMM all-atom additive biological force fields. J Comput Chem 31(4):671–690, PMID: 19575467, https://doi.org/10.1002/jcc.21367.
Venkatasubban KS, Johnson JL, Thomas JL, Fauq A, Cusack B, Rosenberry TL. 2018. Decarbamoylation of acetylcholinesterases is markedly slowed as carbamoyl groups increase in size. Arch Biochem Biophys 655:67–74, PMID: 30098983, https://doi.org/10.1016/j.abb.2018.08.006.
Wang Y, Huang R. 2016. Correction of microplate data from high-throughput screening. Methods Mol Biol 1473:123–134, PMID: 27518630, https://doi.org/10.1007/978-1-4939-6346-1_13.
Wang Y, Jadhav A, Southal N, Huang R, Nguyen DT. 2010. A grid algorithm for high throughput fitting of dose-response curve data. Curr Chem Genomics 4:57–66, PMID: 21331310, https://doi.org/10.2174/1875397301004010057.
Yu W, He X, Vanommeslaeghe K, MacKerell AD Jr. 2012. Extension of the CHARMM general force field to sulfonyl-containing compounds and its utility in biomolecular simulations. J Comput Chem 33(31):2451–2468, PMID: 22821581, https://doi.org/10.1002/jcc.23067.
Zhao YJ, Wang XY, Wang T, Hu X, Hui X, Yan MX, et al. 2011. Acetylcholinesterase, a key prognostic predictor for hepatocellular carcinoma, suppresses cell growth and induces chemosensitization. Hepatology 53(2):493–503, PMID: 21274871, https://doi.org/10.1002/hep.24079.